9-3-2013

Comparing water to DNA for simulation of Auger electron direct damage to DNA using Geant4

Elliott Leonard

Elliott J. Leonard

Candidate

Chemical and Nuclear Engineeering

Department

This thesis is approved, and it is acceptable in quality and form for publication:

Approved by the Thesis Committee:

Cassisano de Olivera , Chairperson

Adam Hecht

Kenya de Almeida

Comparing Water to DNA for Simulation of Auger Electron Direct Damage to DNA Using Geant4

by

Elliott Jacob Leonard

B.S., Nuclear Engineering, University of New Mexico

THESIS

Submitted in Partial Fulfillment of the
Requirements for the Degree of

Master of Science
Nuclear Engineering

The University of New Mexico

Albuquerque, New Mexico

May, 2013

Dedication

To my parents, Rebecca Roh and Andy Leonard, for the encouragement and love needed to complete this degree

To my fiancée, Susan Halbig, for the love and support that only she can give

"My work is a game, a very serious game. "
– M.C. Escher

Acknowledgments

I would like to thank my advisor, Professor Cassiano R. E. de Oliveira , for his support and guidance. I would also like to thank Professor Adam Hecht for providing his knowledge that was often needed. I want to acknowledge David Dixon for helping with cross section sampling. I acknowledge Dr. Robert Busch for his assistance in the writing of this document. Finally, I want to thank my brother Alex Leonard for blazing the trail and sharing his unique knowledge.

Comparing Water to DNA for Simulation of Auger Electron Direct Damage to DNA Using Geant4

by

Elliott Jacob Leonard

B.S., Nuclear Engineering, University of New Mexico

M.S., Nuclear Engineering, University of New Mexico, 2013

Abstract

Typically water is used as an analog material for Deoxyribonucleic Acid (DNA) in Monte Carlo simulations of biological radiation interactions. Prior to this work, it was unclear whether water is an appropriate stand-in for DNA when simulating direct radiation damage on the nano scale. The increased interest in targeted tumor therapy using Auger electrons has requires an understand of the radiobological effectiveness of low energy electrons. A chromatin fiber was constructed within the Geant4 simulation toolkit down to the molecular level. The Binary Encounter Bethe (BEB) model for electron impact ionization was added to the Geant4 Toolkit so the cross sections of molecules could be more accurately modeled. Validation was performed by comparing the BEB model to the *ab initio* Born model already implemented in Geant4. The BEB produces less ionization events but is effective at comparing DNA to water in this context by providing order-of-magnitude similarities in the results. Using the BEB model the number of double strand breaks for DNA was shown to be much greater than for water, indicating that water is not an effective analog for DNA.

Contents

List of Figures **ix**

List of Tables **x**

1 Introduction **1**

2 Background **4**

2.1 Auger Electrons and Radiation Termonology 4

2.2 DNA Structure 5

2.3 DNA Damage and Repair 9

3 Simulation **15**

3.1 Geant4 15

3.2 Physical Model 17

3.3 Geometry 25

3.4 Analysis overview 30

4 Results **31**

4.1 Validation 31

4.2 DNA Simulations 36

5 Conclusion **42**

6 Future Work **44**

6.1 Model Improvements 44

6.2 Other Particles 46

Appendices **47**

A Computer Specifications **48**

B GAMESS Input Files **49**

C Geant4 Geometry Error **52**

References **53**

List of Figures

2.1 DNA Structure 7

2.2 Nuclesome and Chromatin fiber 8

2.3 Lethal Chromosomal Aberrations 12

2.4 Non-Lethal Chromosomal Aberrations 13

3.1 Fundamental Backbone Block 26

3.2 Simulation Geometry 27

3.3 Chromatin Fiber Model 28

4.1 Total Ionizations 32

4.2 Validation Graphs 33

4.3 Total Cross Orbital Cross Section 34

4.4 500 eV Differential Cross Section 35

4.5 DNA vs Water Ionizations 37

4.6 Cross Sections for the Materials 38

4.7 Secondary Energy for DNA vs. Water Graphs 40

List of Tables

3.1 Molecular Properties of The Materials 23

3.2 Material Properties 29

4.1 Strand Breaks 39

Chapter 1

Introduction

The field of small-scale dosimetry has grown with the realization of the potential of biologically significant targets and short range particles for therapeutic applications [23]. The short range of the particles reduces collateral damage to healthy tissue by targeting malignant tissues. The reduction in damage to healthy tissues reduces the patient's risk of treatment. Auger electrons are an ideal candidate for targeted tumor therapy, because most Auger electrons have low energies of ∼20-500 eV with subcellular ranges (∼1-10nm) in biological material [20]. Experiments have shown that the radiobiological effectiveness of Auger electrons is much higher than what is approximated through the widely used Medical Internal Radiation Dose (MIRD) method [13]. On the nanometer scale; the heterogeneities of biological material, the stochastic nature of radiation energy deposition, and the geometry of radiosensitive targets, requires consideration in calculations [23]. As such, the The American Association of Physicists in Medicine (AAPM) formed a task group to investigate the dosimetry of Auger electrons because conventional dosimetry ignores the risk of low-energy electrons [13].

The usage of Auger electrons for treatment requires an intimate understanding of

the damage they cause. Deoxyribonucleic Acid (DNA) is regarded as the molecular target of radiosensitivity [13]. Far from the DNA, Auger electrons typically result in inconsequential dose, as the safety record of nuclear medicine imaging has shown [23]. The range of Auger electrons requires that they are in close proximity to DNA to be effective. Radiation's stochastic nature of interactions and the high non-uniformity of the radiotoxicity of low energy electrons increases the need for the track structure of the electrons. This is done by convention in health and medical physics, were tissue is treated as water. Typically, modeling the DNA geometry is not necessary for bulk calculations, however, Auger emitting isotopes can be incorporated into the DNA and require detailed geometric models [23]. One such incorporated auger emitter is ^{125}I-labled thymidine precursor idodeoxyuridine (^{125}IUdR) which acts like a direct replacement for the thymine base. ^{125}IUdR can be incorporated in the nuclear DNA strand at a thymine location, and has been shown to be even more effective than interlacing an Auger emitter to the grooves of the DNA strand [13]. ^{99m}Tc is another candidate for Auger therapy, it is widely used in nuclear medicine applications already, and can be used for *in vivo* imaging as well [1].

According to Roeske et al. [23]: there is insufficient data to accurately model electron interactions within the DNA, and therefore numerous simplifications are required. One typical simplification is to use water as an analog for DNA material in the geometry of the simulation [2]. It is unclear whether the use of water as the material in the complicated DNA geometry is suitable for molding the effects of Auger Therapy. Using the constituent molecules of DNA would refine the model ensuring that reaction rates of Auger Electrons are accurately represented in simulation models. This work determines if the previous use of water as an analog for DNA material is accurate enough to characterize damage done to DNA through Auger Electron interactions.

The current work is focused on comparing the damage done to DNA, when DNA

is modeled as water or the constituent molecules for low energy electrons on the nanoscale. This comparison serves as a test for the water material analog. Geant4 was used for the simulation, but the available physics models would not allow DNA molecules. A model had to be implemented that could be quickly and easily adapted to different materials. The Binary-Encounter Bethe model was chosen for its simplicity and reasonable accuracy. `GAMESS` was used to calculate molecular orbital information necessary of the physics model. Chapter 2 discusses the structure of DNA, how it is damaged, the implications of damage, and the repair mechanisms. The chapter is intended to give a brief overview of the applicable biology. Chapter 3 derives the implemented physics model and describes the available model already included in Geant4. It also explains the geometrical implementation, cross section sampling, and the strand break algorithm. The results and a discussion is presented in Chapter 4. The final two chapters 5 and 6 make the concluding remarks and describe the work that can be done in the future to increase the accuracy of the work.

Chapter 2

Background

2.1 Auger Electrons and Radiation Termonology

Auger electron emission is a form of atomic deexcitation, which is usually the result of electron capture or internal conversion radioactive decay processes [23]. Electron capture is a result of a proton-rich nucleus capturing an orbital electron. Typically a K-shell electron is captured leaving an inner shell vacancy. The atom is left in an excited state, and deexcites by the outer shell electrons cascading into the vacancies releasing either x-rays or Auger electrons with each transition. Auger emission is more common than x-ray emission, especially with low Z materials [23]. The kinetic energy of the emitted Auger electron is the difference between the orbital energies minus the binding energies. An Auger electron can also be created as a result of internal conversion. An excited nucleus can return to ground state by transferring the energy difference between the ground and excited state to an electron. The electron is ejected and given the energy of the transition minus the binding of the orbital in which the electron was occupying.

Molecular structures can be damaged through ionization, where radiation with

sufficient energy interacts with atomic electrons, imparting enough energy to liberate the atomic electron. DNA is critical molecular structure which is critical to biologic function. Macroscopically, radiation's ability to cause damage is given by radiobiological effectiveness (RBE), which is measured as the damage done from a test dose relative to a reference dose, usually 220 kVp x-ray or ^{60}Co γ-ray [10]. For charged particles, the amount of energy transferred to the medium along a given length, referred to as linear energy transfer (LET), is an important factor determining the RBE. Higher LET radiations impart more energy to radiosensitive areas, such as DNA. Due to the stochastic nature of radiation interactions, imparting more energy in a smaller length increases the chance of damage from depositing energy in DNA [27]. The International Commission of Radiological Protection (ICRP) also defines a radiation weight or quality factor that indicates the radiation's ability to cause damage [27]. Typically, the higher the LET, the higher the quality factor: heavily charged particles (non-relativistic ions) have a quality factor of 20. Low LET radiations: electrons and photons, have a factor of 1[27]. Mass, at higher energies, is a very important quantity in creating radiation damage.

2.2 DNA Structure

Deoxyribonucleic Acid (DNA) is a macro-molecule that contains the encoding for the development and function of all living organisms on Earth. It is composed of a long string of mono-metric units known as nucleotides. The lower right side of Figure 2.1 shows the four possible nucleotides. Each nucleotide, is an assembly of 3 molecular fragments: 2-deoxyribose sugar, a phosphate, and one of four nucleobases. [24]. The nucleobases: thymine, cytosine, adenine and guanine are divided into two groups: pyrimidines and purines. Pyrimidines are 6 member rings (cytosine, and thymine) while purines are fused 5 and 6 member rings (adenine and guanine). The

nucleobases are bound by the first carbon in the deoxyribose sugar to a nitrogen in the base. The sugar and the phosphate make up the structural scaffolding of DNA. The phosphate of one nucleotide is bonded to the sugar molecule of another. Each phosphate is bound to the deoxyribose in the third (3 prime) and fifth (5 prime) carbon. The linked nucleotides form a chain of DNA, with one ending in the fifth carbon (5' end) and the other in the third carbon (3' end). DNA exists as two chains hydrogen-bonded together running antiparallel. At each end of the DNA strand one chain has a 5' end and the other chain has a 3' end. The nucleobases facilitate the hydrogen bonding between the nucleotides of the 2 molecules. To form a stable molecule, there must be at least two "cyclic" hydrogen bonds (N-H$\cdots$O or N-H$\cdots$N) [24]. Due to this restriction and the structure of the bases, guanine can only hydrogen bond to cytosine and adenine can only bond to thymine. This process is referred to as base pairing and provides redundancy in the DNA.

DNA has several layers of structure; the first being the double helix twist of the strand. There are several orientations of the double helix structure that are dependent on the surrounding conditions, however only the B-DNA configuration is being considered in this work. B-DNA is the most common form found in mammalian cellular environments, and is therefore, the most relevant for this work [16]. A double helix geometry leads to a major and a minor grove, which have been shown to have widths of almost 7:4 [32]. With about 10 base pairs per 360° turn and 3.32 Å rise per base pair, the grove widths for the major and minor groove are 22 Å and 12 Å respectively [4]. Figure 2.1 shows DNA including the double helix and the composition of the nucleotides.

Mammalian DNA contains about 2×10^9 base pairs; with each base pair rising 3.32 Å , the total length of the DNA strand is 66.4 cm. Eukaryote cells (general classification of cells that includes mammals) are on the scale of μm, which requires a vast amount of DNA folding to allow it to fit within a cell. 147 ($\pm$ 2) base pairs

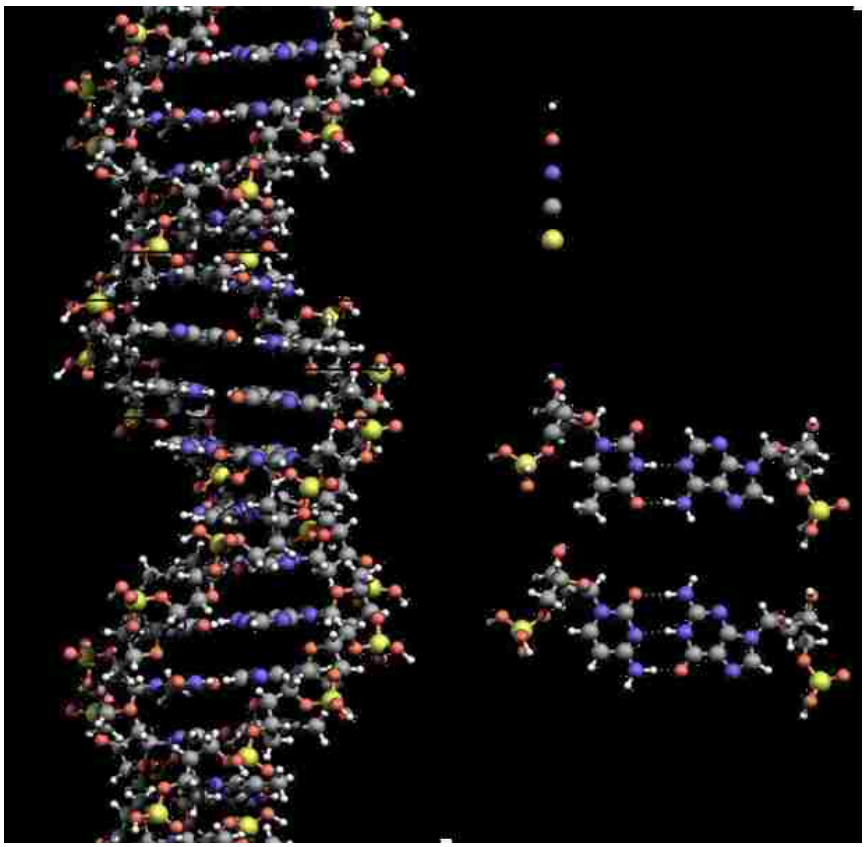

Figure 2.1: A ball and stick representation of DNA. Included are the details of of the nucleotides and and their hydrogen bonding (represented by a dashed line). The major and minor grooves are labeled on the left. The bases are grouped into their respective groups, pyrimidines and purines[30].

are wrapped 1.6 to 1.8 times in a flat, left-handed superhelix around an octomer of 4 core histones (H2A, H2B, H3, H4) [17] . H1 and H5 histones bind the two groups of the core histones and another 20 base pairs to compete a nuclesome. Nuclesomes are connected together through "linker DNA" that consists of 0-80 base pairs [22]. The nuclesomes are then organized into a chromatin fiber, 33nm in diameter with 11 nuclesomes per turn [22]. The fiber is left-handed single start helix. There are other forms of chromatin fiber, but a nuclesome-repeat-length of 197 base pairs is the most abundant, and the left-hand single start is the only way to fulfill such constraints[22]

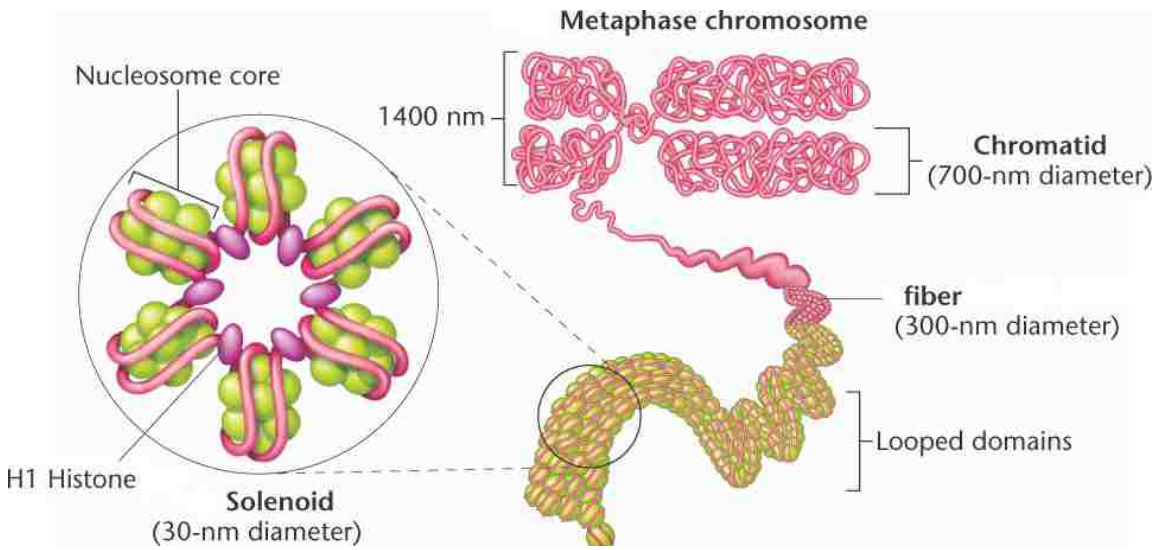

Figure 2.2: 11-nm DNA is packed into a 30-nm chromatin fiber slice called a solenoid consisting of several nucleosomes coiled together. During condensation to the mitotic chromosome, the 30-nm fiber forms a series of looped domains that further condense into a 300-nm fiber. The 300-nm fibers then coil into the chromatid arms seen in metaphase chromosomes. [15]

[31]. Figure 2.2 shows the assembly of the nuclesomes into the chromatin fiber.

For cell division (metaphase), the chromatin fiber will be further organized into a chromosome by more binding proteins. The structure of the chromosome is important because it can affect the viability of the cell [7]. A chromosome contains origins for replication, a telomere, and a centromere [29]. The chromosome is an assembly of chromatids (replicated chromatin assemblies) resembles and 'X' with the centromere serving as the crossing point. DNA replication begins at the aptly named origins of replication where replication proteins are assembled to initiate the process. These sites occur about 30-40 thousand base-pairs apart [29]. A telomere is DNA bound by telomeric proteins located at the ends of the linear chromosome. The telomeres distinguish the natural ends of the chromosome from ends of broken DNA [29]. During mitosis, the two chromatids are pulled into the daughter cells; this requires

machinery (mitotic spindles) to pull on the daughter chromosomes. The site where the spindles attach is a protein complex called a kinetochore. A centromere is the base pair sequence that constructs the kinetochore. The centromere is a very important structure. If it is missing, the chromosomes separate randomly leading to loss of or the duplication of chromosomes as they are not pulled by the spindles to their correct locations [29]. Multiple copies of the centromere creates multiple kinetochres where a single chromosome can be pulled to both daughter cells causing breakage [29].

2.3 DNA Damage and Repair

DNA damage is of interest because it can lead to cell death or mutations through incorrect repair. Single cell death will be of little consequence to multicellular organisms, but mutations can lead to carcinogenesis [10]. The carcinogenesis can result in the organism's death. Understanding DNA damage can lead to understanding of the process of carcinogenesis and radiation-induced cell death.

Ionizing radiation can cause damage in two ways: direct and indirect action. Radiation acting upon the constituent atoms of DNA is referred to as direct action. Damage is caused by deposition of radiative energy into the bonds that bind DNA together. Indirect action is caused by the ionizing radiation interacting with the water surrounding the DNA strand. The ionization of the water produces a free radical (OH^-) that acts chemically upon the DNA strand. Indirect action typically has a time delay (10^{-12}sec. to 10^{-9}sec.) as a result of the radical needing to diffuse to the DNA site [27].

The most important interactions, whether they be chemical or radiological, are to the sugar-phosphate backbone that holds the strand together. When the backbone is damaged the strand is broken. Damage to one of the chains is referred to as a Single Strand Break (SSB), damage to both chains is a Double Strand Break (DSB).

While it is likely after irradiation that the DNA will be damaged on both chains, for a double strand break to occur, two single strand breaks must occur close enough to cleave the DNA into two sections. For ^{60}Co γ rays, there is a ratio of SSB to DSB of about 20:1, and a ratio of direct and indirect action of about 36:65 [6].

DNA damage is not perminate, the cell has pathways in which to repair the damage. Inaccuracies in the repair process are typically what lead to biological effects. Single strand breaks are handled by excision repair, where a damage base, or set of bases are removed and new bases are synthesized [29]. Excision repair requires the strand containing the damaged bases to be broken (as in a SSB event), and the new bases synthesized in the same manner as DNA replication using DNA polymerase. The backbone of the new bases is then joined to the backbone of the existing DNA using DNA ligase [7]. In a SSB, the last step of excision repair is to rejoin the phosphodiester bond. This process is fairly accurate as the undamaged strand can be used as a template for the new bases, and the backbone being of uniform composition is simple to repair [29].

Double strand breaks are much more serious and can lead to structural changes of the chromosome or mutations [7]. The repair mechanisms for double strand breaks depend where the cell is in the cycle, as the presence of a "sister chromosome" (copy of the undamaged DNA) is required for the more accurate pathway [29]. When a "sister chromosome" is present, homologous recombination can occur. This process begins by an enzyme degrading the DNA strand such that single strand (ssDNA) tails exist. The tails then invade the undamaged homologous "sister chromosome" and are synthesized from the 3' ends. The newly synthesized bases are joined to the 5' end, and the DNA has been repaired [29]. If a sister chromosome is not available, early in the cell cycle, the DNA will be repaired through nonhomologous end joining (NHEJ), where the ends of the DNA strand are simply joined together. The misalignment between the two strands protruding from the ends is what facilitates this process.

There only needs to be as few as one base pair of complementary bases [29]. The tails are removed, gaps are filled, and the DNA is said to be repaired. However, as mentioned before, NHEJ is very error prone and leads to the survival of only one yeast cell per 1000 when DSB are introduced [29].

Chromosome aberrations are caused by irradiation early in interphase (time when the cell performs its functions), before the chromosome has been duplicated. Later in the cell cycle, after interphase, there exist two chromatin fibers, which if damaged, are referred to as chromatid aberrations [10]. The types of aberrations are quite extensive and beyond the scope of this document, however, a brief overview of the two major types, lethal and viable, and examples provide insight into the biologic implications of strand breaks. Lethal refers to a mitotic death, where the cell will die during mitosis. A cell may complete several rounds of mitosis before chromosomal damage causes the cell to die [10]. Lethal aberrations are characterized by gross deformations of the chromosome such as, deletions of telomeres or addition or deletion of centromeres. Without the proper structure, four telomeres and one centromere the chromosome will not be able to undergo mitosis without severe damage. Figure 2.3 gives three common examples of lethal chromosomal aberrations. Non-lethal aberrations result in rearranged genetics (mutations), but the structure remains intact, allowing the mutations to be carried into further generations. Figure 2.4 shows three examples of non-lethal aberrations. Mutations from non-lethal damage can lead to malignancies and endanger the organism [7]. A cell has mechanisms for dying used to remove old and damaged cells. If the cell detects chromosomal damage (assuming the damage is not to the diagnostic genes) a cell can undergo apoptosis, programmed cell death, to protect the organism [10].

The structure and composition of DNA is essential to developing simulations. The biologic implications of damage provides an understanding of the outcomes of

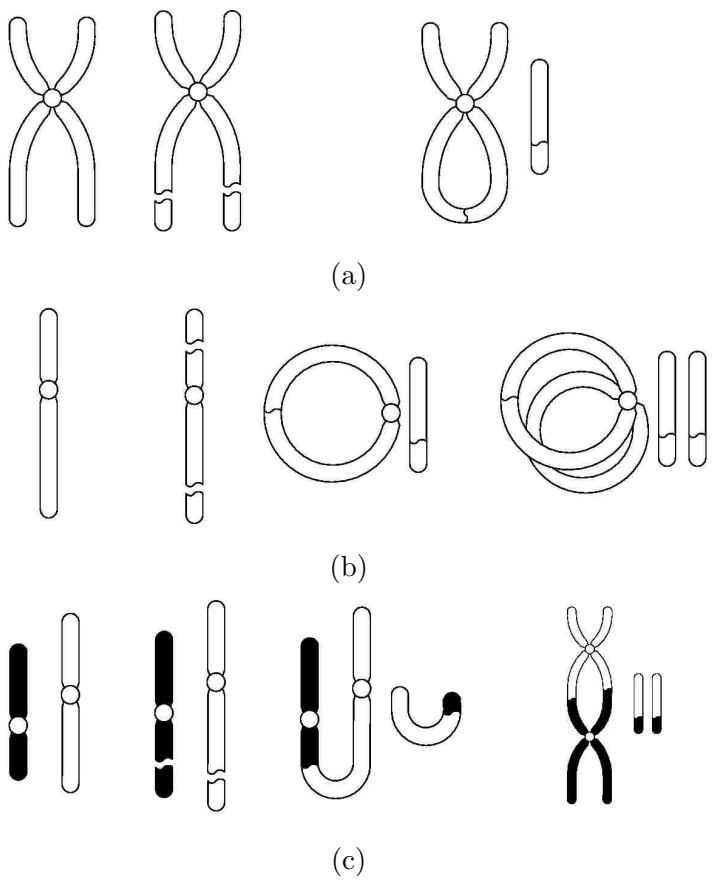

Figure 2.3: A diagram representation of three lethal Chromosomal aberrations. 2.3a shows a normal chromosome with a break in both chromatids. The "sticky" ends rejoin to form the bridge. 2.3b demonstrates the ring type chromatid aberration where a DDS break occurs on both sides of the centromere and rejoins to form a ring and the fragments form an acentric fragment. 2.3c illustrates the process of forming a dicentric chromosome. Two nearby pre-replication chromosomes (represented by black and white) each have a DSB, followed by the two chromosomes join together leaving a acentric fragment. Note the chromosomes are extremely distorted from the a normal chromosome in the first image of 2.3a.

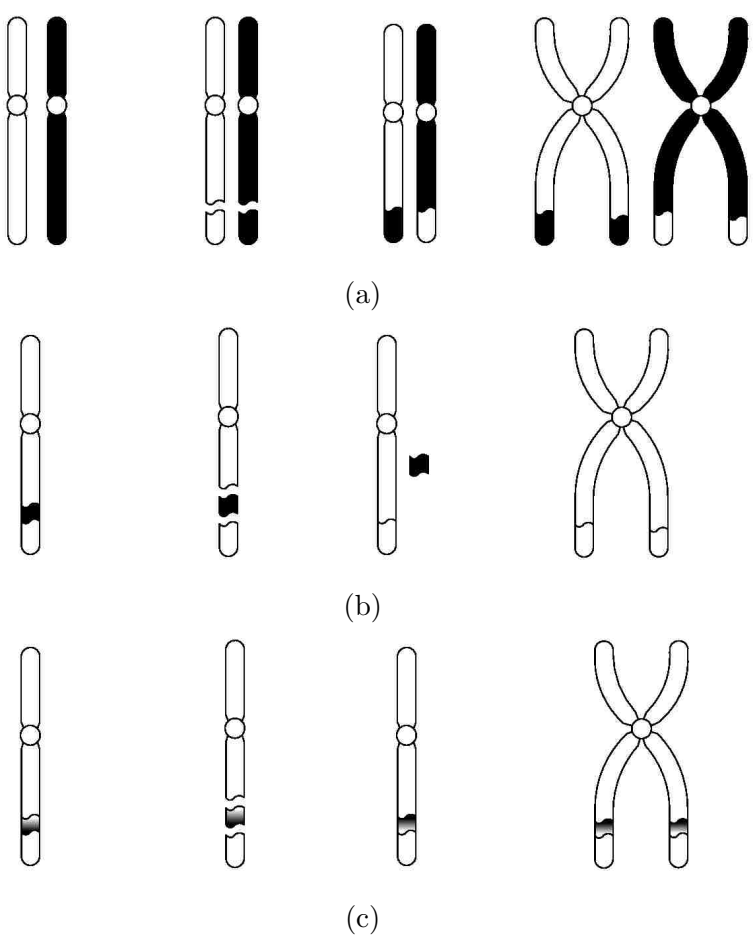

Figure 2.4: A diagram representing chromosomal damage that is potentially viable. 2.4a shows a translocation event where a section of DNA (one or several genes) is switched with a section of DNA from another chromosome. 2.4b demonstrates how sections of DNA are deleted from the genome. Two DDS occur creating a fragment which never recombines with the chromosome. 2.4c illustrates a section of DNA becoming inverted. The shading in the figure represents the directionality of the original DNA fragment. Note how the chromosomes end up without sever distortions and will likely function properly during mitosis.

DNA irradiation. DNA is composed of four nucleobases which contain the genetic information of an organism. The nucleobases are arranged in a long strand held

together by a sugar-phosphate backbone. That strand in folded into a chromatin fiber, which is in turn folded into chromosomes. DNA can be damaged through radiological direct action or radiation induced chemical indirect action. The radiation can be any ionizing radiation, but the focus of this work is on Auger electrons. The low energy Auger electrons are a result of atomic deexcitation. A single ionization in the DNA backbone can result in a strand break. When another strand break occurs on the opposite side near the former, there is a double strand break (DSB). A DSB can be difficult to repair resulting in chromosomal aberrations, that can be either lethal or non-lethal mutations.

Chapter 3

Simulation

3.1 Geant4

The simulations follow the Monte Carlo approach to radiation interactions and transport. Monte Carlo utilizes the the stochastic nature of radiation interactions by simulating the track structure of particles. Essentially, Monte Carlo methods sample Probability Distribution Functions (PDF) to estimate the probability of an event taking place [9]. Since cross sections are PDFs, the use of Monte Carlo is particularly suited for such problems. This methodology does raise issues, because to properly sample a PDF with low probability regions requires numerous samples.

On such simulation package is the Geant4 toolkit. Geant4 was developed at The European Organization of Nuclear Research (CERN) for high energy physics simulations related to the Large Hadron Collider[12]. Unlike most simulation codes, Geant4 is open source, which means the software is available for user modification. This allows for complete transparency, a wide user base, and the ability to change or expand the capabilities. This has lead to development and adoption of the toolkit for many applications including astrophysics, medical physics, and safeguards. Geant4,

written in C++, was an improvement of its predecessor Geant3, written in FORTRAN, as a result of an inquiry on how to adopt modern computing techniques to to the existing program [3]. The first release of Geant4 was in December of 1998, followed by the establishment of the collaboration the next month [3]. The Geant4 collaboration continues development, support and maintenance of the ever growing code package. It was developed with 7 higher level domains:

- geometry and materials,
- particle interaction with matter (physics),
- tracking management,
- digitization and hit management (detector simulation),
- event and track management,
- visualization and visualization framework, and
- user interface [3].

These can be utilized through included, 3^{rd} party, or user-developed interfaces.

Geant4 is not a fully functional simulation package but simply a toolkit, meaning that the end user must write an application tying the physics, tallies and geometries to the foundation dstributed by CERN [3]. This processes is aided by Geant4's utilization of the object-orientated philosophy of C++. The user is given immense power to control precisely what physics models are used, which particles are simulated and how the information is extracted from the simulation. Furthermore, the user may choose to not use the included physics but write his/her own, if the hundreds of models are suitable. The user can still utilize the other physics, the geometry handlers, random number generators, and equally important Monte Carlo functionality

without having to write a standalone code. This can also increase the scope of some problems. Geant4 includes physics for many particles over a very large energy range, thereby allowing more complicated problems to be simulated in depth. All of these properties make Geant4 the ideal candidate for testing Monte Carlo-based physics models. The modularity of the toolkit gives the user, after writing the application, "plug-and-play" capabilities. The physics models inherent from virtual classes that outline the necessary content that will be called by other parts of the program. As long as the physics model is written with the appropriate functionality, Geant4 will adopt it as if it were a part of the release.

3.2 Physical Model

DNA direct strand breaks are caused by an electron dislocation [9] following an inelastic collisions. There are two inelastic collisions with electrons in the low energy range: excitation, and ionization. In both process an incident electron interacts with bound orbital electrons. The incident electron is scattered and energy is transferred to the target electron. The difference lies in the final state of the target electron. Excitation leaves the target election bound to its atom but in a higher energy orbital. The electron can fall back into its vacancy through atomic deexcitation. Electron impact ionization liberates the atomic electron from any bound states. The target electron becomes indistinguishable from the scattered electron but it is customary to call the faster electron the primary scattered electron with the lower energy being the secondary. Both electrons can cause subsequent ionizations if they have sufficient energy to do so. Ionizations are the principal mode of direct damage; electrons are dislocated causing the molecule to break apart.

Many models for cross sections of electron impact ionization have been proposed; they range from analytic to empirical. The analytic cross sections are a result of

quantum mechanical calculations utilizing the inner product between the initial and final states of two electron wavefunctions [18]. Using first order-perturbation theory, the interaction between the bound, incident, ejected and scattered electrons' wavefunctions ($\varphi_b, \varphi_i, \varphi_e, \varphi_s$ respectively) can be described as

$$M_d = \left\langle \varphi_b \varphi_i \left| \frac{1}{r_{1\,2}} \right| \varphi_e \varphi_s \right\rangle \tag{3.1}$$

where the transition operator is the Coulomb potential. The free electron wavefunction with momentum $\vec{p}$ is an expansion of eigenfunctions and takes the form

$$\varphi(\vec{p}, \vec{r}) = \sum_{lm} a_{lm} Y_{lm}(\theta, \phi) F_l(\vec{p}, r) \tag{3.2}$$

Where $Y_{lm}(\theta, \phi)$ is a spherical harmonic corresponding to the orbital and azimuthal quantum numbers l and m respectively. $Y_{lm}(\theta, \phi)$ is simply the solution to the angular Schrödinger equation. The radial solution $F_l(\vec{p}, r)$, is more complicated as it depends on the applied potential $V(r)$. There are three standard approximations when describing a free electron: Plane Born Wave, Coulomb, and Distorted Wave [18]. The Plane Born Wave approximation sets the potential to zero and completely ignores the target. The Coulomb approximation sets the potential to the nuclear charge (Z) scaled by the separation between the target and the free electron ($^1/_{\vec{r}}$). Typically nuclei do not sit without atomic electrons, as the Coulomb approximation assumes. The Distorted wave accounts for charge shielding and the addition of atomic electrons to the target[18]. With the interaction matrix, the cross section for incident energy (T)and secondary energy of the ejected electron (W) can be derived by summing the interaction probability over L, the angular momentum eigenvalues for the whole system to give

$$\frac{d\sigma(W,T)}{dW} = 16\frac{a_0^2}{T} \sum_L (2L+1) |M_d|^2 \tag{3.3}$$

with the total cross section being integrated over the ejected electron energy. Giving

$$\sigma(T) = \int_0^{\frac{1}{2}(T-I)} \sigma(T,W)\, dT_e \tag{3.4}$$

where I is the ionization energy [18].

Quantum cross sections pose problems for simulations. Monte Carlo, as applied to radiation transport, requires a classical treatment of the particles. The transport equation is linear, and the superposition principal is essential for Monte Carlo tallies. Also the cross sections are typically not easy to calculate, especially for complicated materials where the potential is difficult to calculate. These make the quantum calculations for cross sections acceptable for limited applications. Geant4 already uses The First Born Approximation (FBA) model with corrections for k-shell interactions and low and high energy electrons [28]. These calculations can be very complicated and consume a vast amount of time for even simple molecules such as water. The Geant4 FBA cross sections are tabulated only for water, which is a major limitation when simulating low energy electron interactions. There are many materials that are of interest when studying electrons in any energy regime. There has been a lot of work to generalize the theories for a broad class of atoms, molecules and energies [18]. One such effort was performed by Kim and Rudd where they develop a Binary-Encounter-Dipole model for cross sections [14].

Binary-encounter models are an extension of the Mott cross section, which is a generalized version of the Rutherford cross section [14]. Rutherford cross sections describe the collision of a particle of charge Ze with a free electron at rest. Mott was able to generalize the cross section to account for the collision of two electrons. The Mott cross section can be modified to account for bound electrons by taking into account the binding energy of the shell (B) and the number of electrons occupying the shell (N). The modified Mott cross section is given by

$$\frac{d\sigma\left(W,T\right)}{dW}=\frac{4\pi a_0^2R^2N}{T}\left[\frac{1}{\left(W+B\right)^2}-\frac{1}{\left(W+B\right)\left(T-W\right)}+\frac{1}{\left(T-W\right)^2}\right] \tag{3.5}$$

where R is the Rydberg energy and a_0 is the Bohr radius[14]. Accounting for the fact that bound electrons are moving within the orbital leads to the binary-encounter model. This is done by associating a momentum distribution to the bound target

electron represented by the average kinetic energy, U, defined as [14]

$$U \equiv \frac{\langle \vec{p}^{\,2} \rangle}{2m}. \tag{3.6}$$

These cross sections are more convenient to express in terms of the reduced variables and a summation. Defining:

$$t = \frac{T}{B} \tag{3.7}$$

$$w = \frac{W}{B} \tag{3.8}$$

$$u = \frac{U}{B} \tag{3.9}$$

$$S = 4\pi a_0^2 N \left(\frac{R}{B}\right)^2 \tag{3.10}$$

we can rewrite the single differentiable cross section in terms of a generalized summation taking the form[14]

$$\frac{d\sigma\,(w,t)}{dw} = \frac{S}{B\,(t+u+1)} \sum_{n=1}^{3} F_n(t) \left[\frac{1}{(w+1)^n} + \frac{1}{(t-w)^n}\right]. \tag{3.11}$$

This form exposes the physical significance of each term. The $(w+1)$ terms account for the energy given to the secondary electron while the $(t-w)$ terms account for the energy lost by the primary electron. $n=1$ describes the interference between the primary and secondary electron, while $n=2$ represents close collisions. The $n=3$ terms arise from the broadening of the energy distribution due to the momentum of the bound electrons [14]. By varying the F_n functions, the model is also varied. The binary-encounter models are given by

$$F_1 = -\frac{1}{t+1}, \qquad F_2 = 1, \qquad F_3 = \frac{4u}{3}. \tag{3.12}$$

When integrated from $w=0$ to $w=\frac{(t-1)}{2}$, equation 3.11 with 3.12 gives the total cross section. However, when t becomes large, the cross section exhibits asymptotic

behavior, which does not agree with predictions from the Bethe theory or experiment [14]. To correct for this, Kim and Rudd [14] developed the Binary-Encounter-Dipole (BED) model. Following the asymptotic cross section derivations by Bethe using the FBA, they take into account the differentail oscillator strength represented by $\frac{df(w)}{dw}$. They go on to define

$$N_i \equiv \int_0^\infty \frac{df(w)}{dw} dw, \quad M_i^2 = \frac{R}{B} \int_0^\infty \frac{1}{w+1} \frac{df(w)}{dw} dw, \quad Q = \frac{2BM_i^2}{NR}. \tag{3.13}$$

The correction for the asymptotic behavior leads to F_n being

$$F_0 = \frac{\ln t}{N\,(w+1)} \frac{df(w)}{dw}, \qquad F_1 = -\frac{F_2}{t+1}, \qquad F_2 = 2 - \frac{N_i}{N}. \tag{3.14}$$

Equation 3.11 can be used but the sum runs from $n = 0$ to $n = 2$ to ensure the $t - w$ term is ignored in the asymptotic region (i.e. when $t \gg w$) as $t - w$ will simply approach t as t becomes larger.

Differential oscillator strengths are often difficult to obtain, particularly for each subshell [14]. Some molecules have simple shapes for the differential oscillator, which can be represented with inverse polynomials. Doing this changes M_i^2, N_i and Q into simple forms [14]

$$N_i = b, \qquad M_i^2 = \frac{RN_i}{2B}, \qquad Q = \frac{N_i}{N} \tag{3.15}$$

where b is a constant. This form further simplifies the BED model into the Binary-Encounter-Bethe (BEB) model. This is model used in this work of calculations for electron impact ionization. It is in the same from as Equation 3.11 but with different F_n functions, which are given as [14]

$$F_1 = -\frac{2-Q}{t+1}, \qquad F_2 = 2 - Q, \qquad F_3 = Q \ln t. \tag{3.16}$$

The BEB model can be further simplified by setting $Q = 1$, for situations where M_i^2 is not known [14]. This approximation will lead to cross sections of the correct order

of magnitude and are very useful when the molecule is complex or nothing is known about the differential oscillator strength.

The total cross section is determined by integrating Equation 3.11 with 3.16 from w to $\frac{t-1}{2}$ to give [11]

$$\sigma(t) = \int_0^{\frac{t-1}{2}} \frac{d\sigma(w,t)}{dw} dw = \frac{S}{t+u+1}\left[\frac{\ln}{2}\left(1-\frac{1}{t^2}\right)+1-\frac{1}{t}-\frac{\ln t}{t+1}\right]. \quad (3.17)$$

Kim and Rudd have shown good agreement of the BEB model with experiments over many atoms and molecules including water [11] [14]. Within the energy range of $10\,eV$ to $10^6\,eV$, the model was particularly good at reproducing cross sections for hydrocarbons, which is ideal for application to DNA. While the BEB model can produce accurate singlely differential cross sections, the BED model produced better energy distributions [11]. As this current work is a proof of concept, accuracy is not of the utmost importance; as long as all the cross sections are produced through the same method, they will serve the purposes of this research.

The angular distribution is less well known [9]. Therefore, the deflection of the secondary electron was calculated kinematically. For higher energies ($> 200eV$) the assumption is that the incident electron collided with a free electron, "ejecting" the free electron at some angle θ. The result of the simple calculation is given by

$$\cos\theta = \sqrt{1-\left(1-\frac{T}{W}\right)\left(1+\frac{W}{2m_{e^-}c^2}\right)^{-1}} \quad (3.18)$$

where $m_{e^-}c^2$ is the electron rest mass in eV. For energies between $50eV$ and $200eV$, the electron is ejected with an average of 45^o. Energies below $50eV$ see isotropic ejection.

The values for B, U,[1] and N used in the Binary-Encounter models were calculated using the General Atomic and Molecular Electronic Structure System (GAMESS).

[1]It is important to note that the value of U is only a theoretical value and has no physical meaning. Its importance comes from a classical treatment of the target election.

Table 3.1: The Molecular properties of the electrons in the molecular orbits of the materials used. This values are taken from the output from GAMESS. The orbits are all doubly occupied as a result of the use of the Restricted-Hartee-Fock method.

H_2O		**Phosphate**		**2-dexoribose**	
B (eV)	U (eV)	B (eV)	U (eV)	B (eV)	U (eV)
559.29	1674.1	2182.4	6322.4	559.90	1673.7
36.961	88.330	561.50	1673.6	559.44	1674.1
19.350	88.330	561.50	1673.6	559.03	1673.9
15.344	109.73	561.40	1673.9	307.82	904.60
13.720	109.73	558.97	1676.8	307.54	904.82
		210.72	710.99	307.28	904.66
		153.50	710.79	307.05	904.61
		153.46	710.63	306.11	904.66
		153.43	710.63	38.164	111.25
		41.519	89.600	37.593	88.518
		39.160	89.600	36.812	88.198
		38.923	89.334	29.426	48.203
		36.646	103.04	28.349	50.109
		24.705	97.365	24.868	50.042
		22.047	97.785	22.817	49.886
		20.694	97.365	22.177	50.191
		18.909	108.59	19.881	95.988
		18.395	108.59	19.021	64.904
		18.082	109.00	18.079	95.123
		16.610	109.00	17.772	49.936
		15.551	108.87	17.328	49.983
		15.146	102.48	16.770	110.61
		15.121	108.87	15.715	64.114
		13.344	94.762	15.687	95.394
		13.230	103.04	15.094	63.484
				14.784	110.29
				13.951	48.534
				13.415	110.77
				12.729	111.25
				12.267	64.479
				12.044	110.38
				11.314	95.439

GAMESS performs *ab initio* molecular quantum chemistry [25]. While able to calculate orbital wavefunctions through many methods, the Restricted Hartee Fock (RHF) method was used for the obtaining B, U, and N. Briefly, the RHF method approximates a N-body wave function (molecular orbitals) with a single Slater Determinate. The restricted aspect assumes a molecule is a closed-shell with all orbitals doubly occupied. The orbitals are approximated as a linear combination of Gaussian-type orbitals, which are similar to Slater-type but are computationally much faster [25]. This current work used a 6-311G Pople basis set, meaning 6 primitive Gaussians were used for the core atomic orbital functions. The valance orbitals were composed of three bases function each; the first bases functions contain a linear combination of 3 functions, while the other 2 bases functions have 1 function each. The values for B, U, and N can be found in Table 3.1. The first molecular orbital corresponds to the S orbit of the oxygen, carbon, or phosphorous which results in the high energies reported. Examples of the GAMESS input files for the three materials are listed in Appendix B.

Equation 3.11 with 3.17 is not an invertible function, meaning that direct Monte Carlo sampling is impossible. The single differentiable cross section must be sampled by rejection; where the cross section probability density function (PDF) is bound by an easily invertible PDF. The bounding function is inverted and normalized to a cumulative distribution function (CDF); the CDF is sampled to obtain an independent variable; in this case the reduced secondary energy. The dependent variable is multiplied by a random number; if the result is greater than the cross section the value is rejected and the CDF is sampled again. The process repeated until the independent variable multiplied by a random number falls below the value of the cross section. Because the cross sections must be sampled many times, efficiency is essential. The choice of the bounding function can greatly affect efficiency. The ratio of the area under the cross section to the area under the bounding function should be minimized, however, the bounding function must always be greater than

the cross section. The choice for the bounding function is important; in this work the bounding PDF takes the form

$$g(w) = \frac{\frac{d\sigma}{dw}(0)}{\left[\frac{d\sigma}{dw}(0)\right] w + 1}. \tag{3.19}$$

The bounding function is easily invertible, and provides a good ratio of areas without getting into very complex mathematical theory.

3.3 Geometry

Simulating direct damage to DNA requires a DNA strand to be constructed within the simulation. Monte Carlo handles materials in a way that is not ideal for nanometer length scales. Geometry is modeled as a homogenous material with no molecular structure, with a single number density and corresponding interaction cross section. In the case of electron impact ionization, the ejected electron is essentially created from nothing, and the material remains unchanged. There is no tally for the number of electrons in the material (this would be far too computer intensive). This implies that even if the model is on the nano scale, the molecules must be modeled as "chunks" of that molecule. To do this, a rough volume of the molecule must be calculated, and its shape approximated by a primitive volume. In this case, the volume was chosen to be a prism, a cylinder with angular sides. The dimensions of the prism follow closely to that outlined by M.A. Bernal and J.A. Liendo [2]. There are some key differences between Bernal and Liendo's model and the model implemented in this work. Most importantly is the backbone (phosphodiester) of each base. In their work [2] the phosphodiester is one prism, while in this work the 2-dexoribose and the phosphate are broken up into separate prisms that will be referred to as a phosphodiester Unit (PU). This was done due to computational restrictions with `GAMESS`; when the molecules become too large `GAMESS` would not converge. The dividing of the backbone into two constituent molecules was a work around for this issue. The

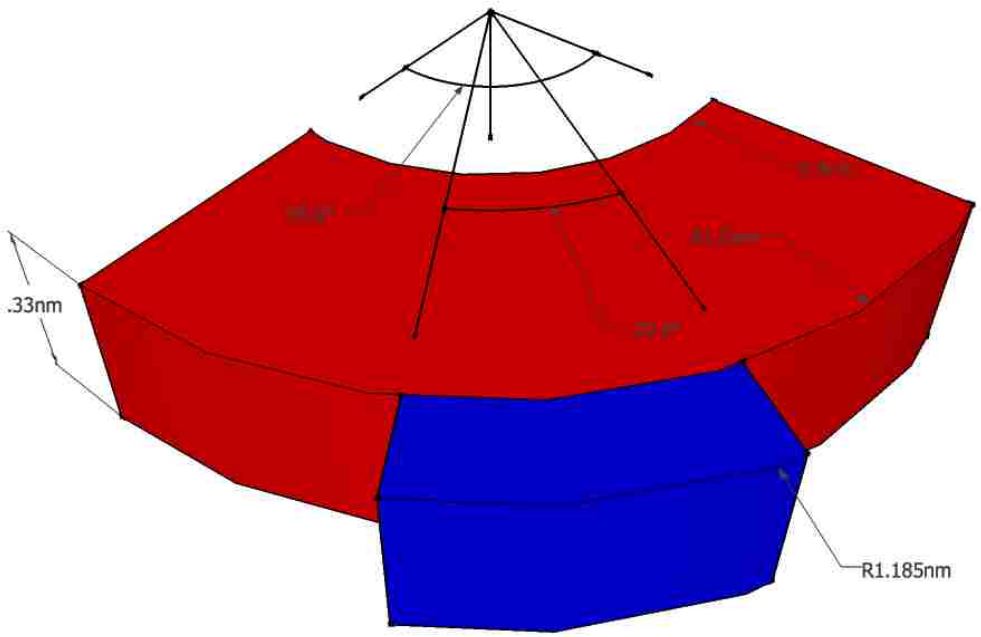

Figure 3.1: A rendering of the fundamental building block for the DNA model, a phosphodiester unit (PU). The Red, inner, prism is the 2-deoxyribose sugar and the blue, outer, prism is the Phosphate

volume of 24.0 Å^3 and the outer radius of 1.185nm were maintained, but the shape was changed slightly. The shape and dimensions of the fundamental building block of the DNA backbone are shown in Figure 3.1. The height of 0.33nm is derived from the rise per base pair of B-DNA [4]. The aperture angle and radius of the prisms were chosen to maintain the overall outside diameter of the DNA strand and the volume of 24.0 Å^3. The aperture angle of 95.0^o for the 2-deoxyribose was varied to give a reasonable aperture angle for the phosphate of 29.6^o. The area from the center line to the beginning of the prism is void to allow for the nucleobases. Other work ([2], [12]) includes the base-pair as cylinders with a radius of 0.5nm and a height

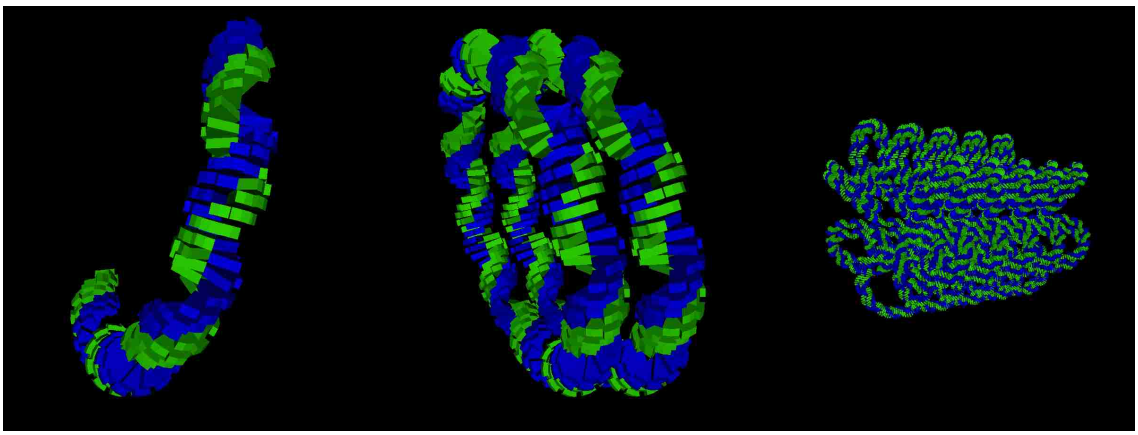

(a) DNA Strand (b) nucleosome (c) Chromatin Fiber

Figure 3.2: The assembly of the basic phosphodiester unit into a DNA strand. The strand makes a complete circle and is copied to make a nucleosome. The nucleosomes are assembled into a hexagonal spiral to make a chromatin fiber.

of $0.33nm$. After repeating the primitive solids in Figure 3.1 numerous times, the memory requirements for the geometry would be quite intensive. Damage to the base also does not result in strand breaks. Therefore, the decision was made to neglect the bases pairs, leaving the area void and subject to the properties of the mother volume.

The PU in Figure 3.1 was assembled into a chromatin fiber through the use of the `G4AssemblyVolume` class to create the geometry in Figure 3.2. The figure indicates that the prism extends to the centerline; this is simply a artifact of the visualization that is unable to construct void at the center of a prism. This class allows the user to assemble smaller volumes into a larger unit that can be easily placed. In this case, 200 PU were assembled into a double helix that wraps into a full circle creating half of a nucleosome. The DNA strand was built by creating the double helix around a circular centerline in the $x - z$ plane with a diameter of $12.37nm$ which allows 100 base pairs or 200 PU. Building the helix required placing units in a rotating reference

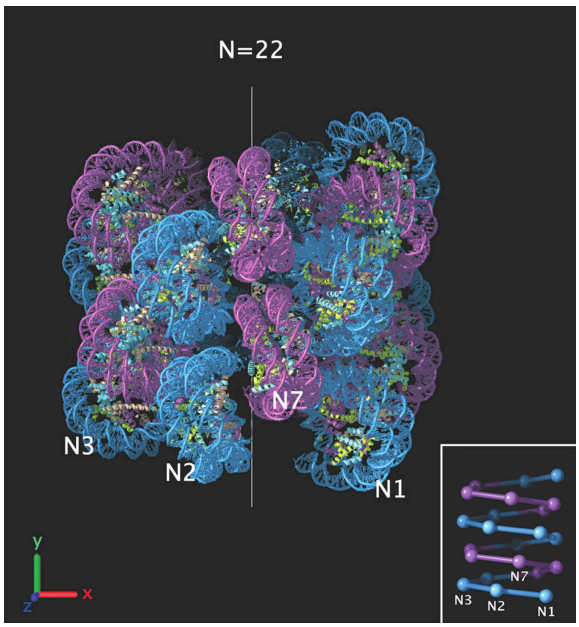

Figure 3.3: The model of a chromatin fiber that the simulation geometry is modeled from[22].

frame and translating it to the Cartesian coordinates native to Geant4 geometry. To begin, two PU were placed with their centers (centerline of the prism and half height) and their "z" axis tangent to the $12.37nm$ circular centerline and in the same plane. They are placed at a polar offset of 9.92^o. Another set of PUs are placed at a polar offset of 3.6^o and rotated about the centerline 35.9^o to give the 10 bp per turn [4]. This is done 100 times to create a half of a nucleosome, which can be moved and copied as an assembly.

A nucleosome as shown in Figure 3.2b is created by taking two assemblies of PUs and stacking them along their centerline axis. The spacing between them is minimal ($< 1nm$), and the histone proteins are simply modeled with void. As the `G4AssemblyVolume` can not make an assembly of an assembly, each half of a nucleosome had to be placed independently when constructing the chromatin fiber. The geometry of this work also differs from other work in the chromatin assembly. Pre-

Table 3.2: The properties of the materials and the volumes they occupy used in the Geant4 simulation. The density of the 2-deoxyribose and the phosphate are based on the mass of the molecule placed into the volume. The density of water is based on bulk properties of water, used in already implemented Geant4 physics.

Molecule Name	Chemical Formula	Molecular Mass ($^{g}/_{mol}$)	Primitive Volume (nm^3)	Density ($^{g}/_{cm^3}$)
Water	H_2O	18.015	0.2400	1.0000
2-deoxyribose	$C_5H_{10}O_4$	118.432	0.2055	0.9546
Phosphate	PO_4H_3	97.994	0.0345	4.7166

vious efforts ([2], [12]) placed the nucleosome such that the centerlines would create a hexagon. The hexagons were stacked in layers to create the chromatin fiber. This work follows the work of Robinson et. al. [22] where the nucleosomes are assembled in one start helix, which greatly increases the packing ratio. Figure 3.3 shows the model that is the basis for this work. The nucleosomes are tilted off-vertical 34^o and a rotation of 6 nucleosomes has a pitch of $9.8nm$. This leads to an outside diameter of $39.58nm$ which corresponds well to the largest measured diameter of $\approx 44nm$ [22]. The simulation utilizes a 60 nucleosome long chromatin fiber, which corresponds to 10 rotations. An example of the chromatin fiber implemented can be found in Figure 3.2c, which is 5 rotations long, half of the implemented length. The entire chromatin fiber is contained within a cylinder of radius of $25nm$ and $120nm$ high. This cylinder is the boundary where the high fidelity physics is activated; it is surrounded by a cube with sides measuring $1.5\mu m$.

The cube and cylinder are water filled and roughly represent the nucleus and water surrounding the DNA strand respectively. These areas are filled with water from the NIST libraries in Geant4, and has a density of $1^{g}/_{cm}$. The PU can be one of two materials: water or phosphodiester. The water-filled PUs have the same water as the surrounding structures. When simulating actual DNA, the phosphodiester unit is filled with one phosphodiester molecule. The molecule is of course divided into the 2-dexoribose, which fills the red area (outer prism) of Figure 3.1, and the phosphate,

which fills the blue area (inner prism) of Figure 3.1. The number density of the PU subunits were calculated using the molecular mass of the respective molecule and the volume of the prism containing the molecule. Table 3.2 shows the properties of the materials used in the simulation.

3.4 Analysis overview

The Geant4 simulation package gives the user vast ability to extract information from the simulation. This instance, requires information from the ionization process, and the areas in which it occurs. For the verification and validation simply the number of ionizations and the information about the scattered and ejected electrons is needed. The strand break simulations require much more geometrical information. A strand break occurs in any PU that experiences and ionization event. Other methods only use energy deposited which includes excitation. Excitation, as mentioned above, does not directly lead to strand breaks. Only ionizations that occur in unique PUs were added to the strand break count. It is possible for an electron to cause two ionization events in the same PU, which does not lead to extra strand breaks. While it was possible for multiple ionization events to occur in the same volume, they do not cause an extra strand break. A double-strand break was said to occur if two ionization events occurred on opposing strands within 10 base pairs. While it is possible for single-strand breaks to cause a double-strand break, this phenomenon occurs so infrequently that it can be neglected [6]. The DSBs must be counted at the end of every event (birth and death tracking of a particle) and not at the end of a run (all the events). The event level processing mimics natural conditions, where a single particle is emitted causing damage. The simulation resets and another particle is launched, tracked, and the damage counted. This repeats for the total number primary events in a run.

Chapter 4

Results

4.1 Validation

Validation was performed by comparing the physical models in Geant4 to the implemented model. Typically simulations need to be compared to experiments, but the limited scope of this work has made finding experiments to simulate particularly problematic. In an experimental setting, it is very difficult to separate damage done to DNA in water via direct and indirect action [26]. One solution is to dehydrate the DNA via a vacuum, but this leads to other issues. Water is still present up to 10% of the weight of the DNA by binding to the phosphate group [26]. Overlying salt also contributes to to the shielding effects of electrons impinging on "dry" DNA. It was found that the salt that prevented denaturing could not be removed to less than a ratio of 1:1 of DNA to salt by weight, as it would result in DNA damage [5]. All of these factors would be computationally very difficult to include; the result would be a meaningless comparison. The salt addition would add to the already expensive computations, and the water contributes indirect damage to DNA that cannot be accounted for in the current model. The geometry of the experiment used

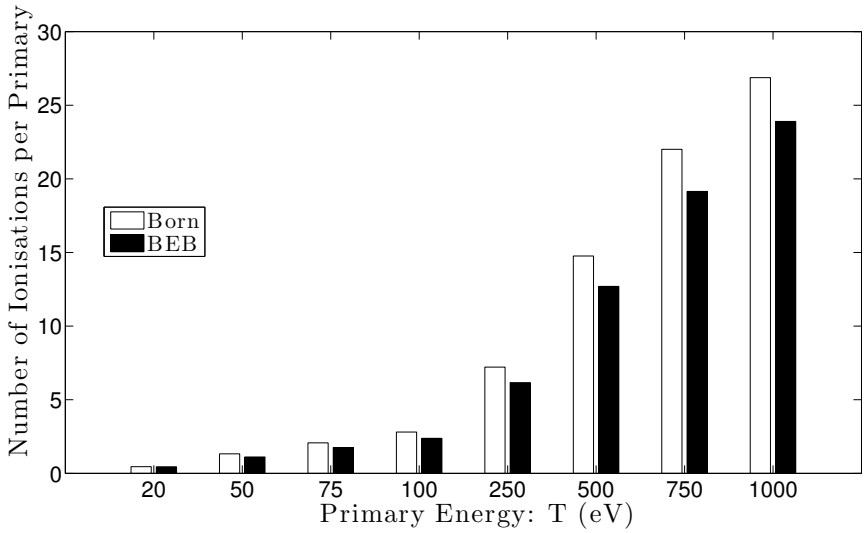

Figure 4.1: The total number of Ionization events that occurred during the validation run. The chart shows the comparison of the ionizations from the Born model available in Geant4 and the BEB model implemented for this work.

a pBR322 supercoiled plasmid, which would require a complete redesign of the supercoiled geometry implemented in this work [5]. Such efforts are beyond the scope of this project.

Comparing the total number of ionizations from each model in a water volume evaluates the ability of a particular energy electron to cause ionizations. Figure 4.1 shows the total number of ionizations for both models. 1×10^6 elections at each energy were run which gives a statistical uncertainty of 0.1%. The total number of ionizations from the BEB is consistently smaller than that of the Born. The difference grows as the energy becomes larger. The total cross section for the Born and the BEB model are nearly identical, which indicates the difference does not arise from the incident electrons. The primary electrons are equally likely to produce ionizations over other processes for all energies.

Figure 4.2 shows the energies of the scattered and ejected electrons for different

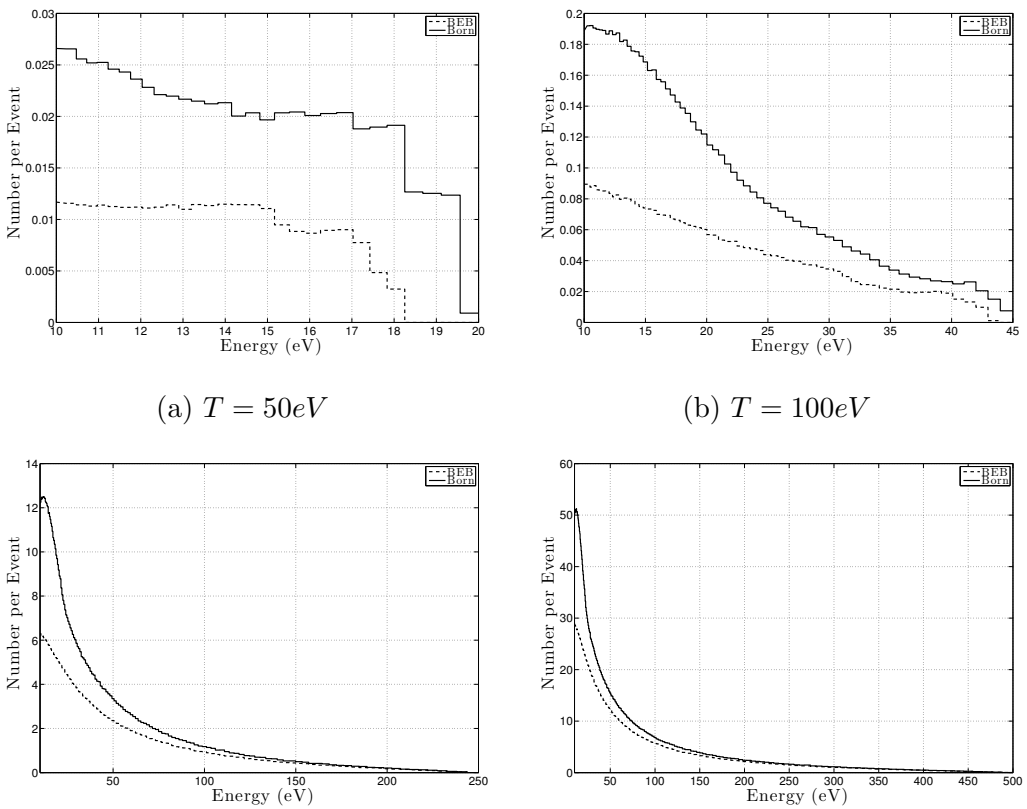

(a) $T = 50eV$ (b) $T = 100eV$

(c) $T = 500eV$ (d) $T = 1000eV$

Figure 4.2: The energy of the secondary electrons, scattered and ejected, from the two models at primary energies of $50, 100, 500$ and $1000eV$. The values have been normalized to the number of primary electrons at that energy

incident energies. It is clear that the BEB model produces lower energy electrons than the Born model. The area under the BEB curve is much smaller than the area under the Born curve; this indicates that the the BEB model gives less energy to the secondaries overall. The only way this is possible is the BEB model is causing ionizations in tighter bound shells than the Born model. Thus, the BEB model must deposit more energy to liberate the electrons in an ionization event. This can easily lead to the discrepancy seen in Figure 4.1. The electrons have less energy after an average ionization event; thus, the scattered and ejected electron have less potential

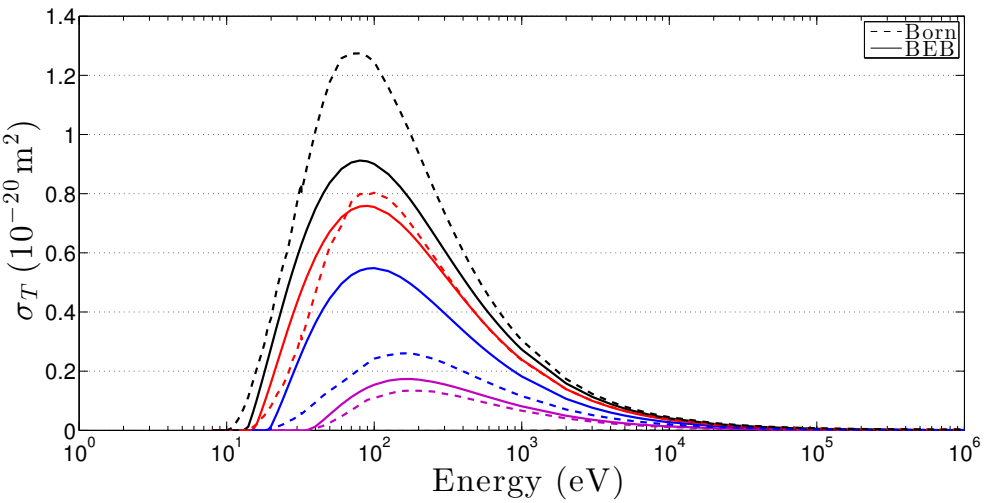

Figure 4.3: The total cross section for water for each orbit as a function of the incident election energy for both the BEB and Born Models. Each color represents a different molecular orbital: black = $1b_1$, red = $3a_1$, blue = $1b_2$, magenta = $2a_1$

ionization events. Figure 4.3 shows the total cross sections for each of the molecular orbits of water. The most probable orbit ($1b_1$) has the lowest binding energy, making the energy given to the secondary electrons maximum. The $1b_1$ and the $1b_2$ orbitals are the source of the discrepancy. For the $1b_2$, the BEB models give a much larger cross section than the Born; with a binding energy of $19.350eV$ versus the $13.720eV$ for the $1b_1$ a significant energy discrepancy can be seen. At the peak, $\approx 900eV$, the Born model produces $\approx 1.5\times$ the probability that the BEB model produces for the $1b_1$ orbit. At the same energy, the BEB model for the $1b_2$ orbital shows $\approx 1.5\times$ higher probability than the Born. Given a significant number of ionizations the Born model will produce more $1b_1$ ionizations giving $13.720eV$ to the volume for electron liberation, while the BEB model will produce more $1b_2$ ionizations giving $19.350eV$ to the volume. Over the course of the simulation, this difference compounds giving the large discrepancy in Figures 4.1 and 4.2.

Another source of discrepancy comes from the differential cross section, which is

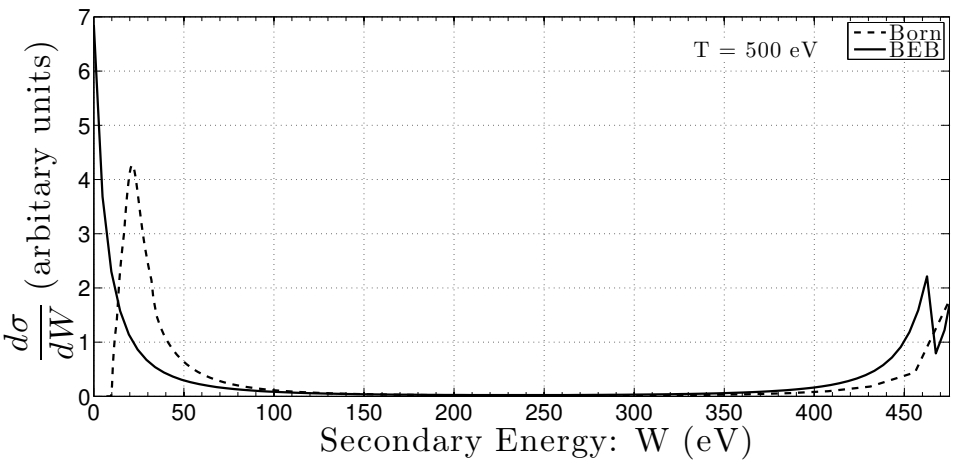

Figure 4.4: The water differential cross sections for the Born and BEB models at incident energy of $500eV$. The BEB is peaked at the low energies while the Born does not allow energies below $8eV$. This indicates that the BEB model produces more lower energy electrons.

displayed in Figure 4.4. For $500eV$ incident electrons, the differential cross section for the BEB model is shifted to lower energies. The Born model produces a spike at about $25eV$, the BEB has the highest probability of zero energy electrons. While the zero energy elections are not physical, this is accounted for by the random number generator, which never produces 0 as a random number. The cross section for the BEB has been artificially extended past its operational limit of $\frac{1}{2}(T - B)$ to show comparison to the Born. According to the models, the scattered electron receives the remaining energy after the electron is ejected and freed from the orbital. The ejected electron from the BEB will have likely have less energy than electrons ejected in the Born model. The scattered BEB electrons will recover that energy but "spend" it on freeing electrons from lower orbits, which accounts for the smaller amount of energy given to the ejected electrons. As was mentioned prior, the BEB model produces order-of-magnitude differential cross sections that are more suited for total cross sections. As the results are relative to water, the cross sections serve the purpose for

this work.

To validate the strand break algorithm, the work by Grosswendt shows the direct action double strand breaks as calculated through global doses to sensitive targets [9]. Grosswendt shows from a $523eV$ Auger electron there are 1.50% DSB to SSB. The single strand break is calculated by assuming a cell nucleus receives $1Gy$. With the mass of the backbone assumed to be $1.7pg$ and 1.36×10^4 ionizations in the nucleus, there are about 360 single strand breaks $/cell/Gy$ [9]. While this is a gross oversimplification of the process, it serves as a guide for calculating the strand breaks in the volume. The simulation volume is smaller than the calculation volume and receives more energy in a much more targeted way. As a result the number of DSBs is larger in the simulation, giving a ratio of $(6 \pm 4)\%$. This puts the number of DSBs on the same order of magnitude, as calculated by Grosswendt. This indicates that the program is functioning correctly, and the physics is adequate for the purposes of this work.

4.2 DNA Simulations

The simulations were carried out using `GEANT4.9.6` on a Mac Pro running `OS X 10.8.3`. More information on the system is listed in Appendix A. The geometry used both water and the DNA in the phosphodiester units. For each electron energy, 1×10^6 events were run. While typical Monte Carlo simulations can run into the billions of events, this simulation had two limitations. When running higher energies, the simulation would hang, refusing to continue. This was caused by an issue with the way Geant4 handles the assembly volume. The error output can be seen in Appendix C; it manifests as a geometry overlap. All of the tools in Geant4 were used to ensure no overlaps. The PUs were so small that electrons would get stuck in or in between a PU, with the space so small, the program could not resolve the volume

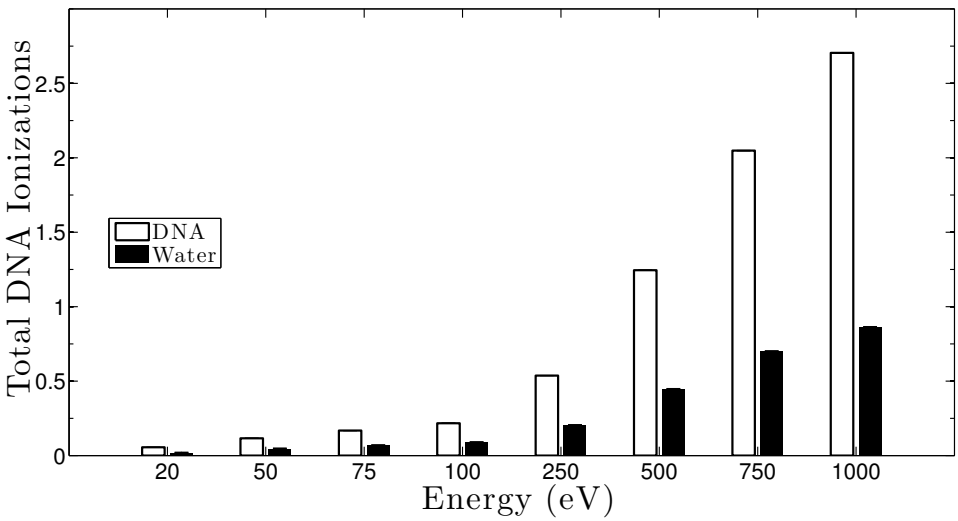

Figure 4.5: The total number of ionizations in a phosphodiester unit per event for the water analog and the DNA materials.

where the particle resided. The PU would meet at an edge causing unresolvable points. This caused the electron to scatter indefinitely. The other limiting factor was time; analog Monte Carlo is very time intensive, especially when the geometry is large enough to contain every electron and they do no leave. This means that they must track the particles until their energy falls below a certain threshold. This can add time to the simulations. The simulation was carried out in "run parallelism" where anywhere from 2-12 instances of Geant4 were run at any one time. The higher energy simulations ($> 500eV$) were broken into 4 simultaneous simulations of 250,000 events.

Figure 4.5 shows the total unique ionizations in the phosodiester units for water and DNA per event. Each unique ionization in a PU represents a strand break, there is a significant difference in the strand breaks between DNA and water. The DNA material resulted in nearly 3× more strand breaks than the water. This could be a result of the larger number density or the differences in cross section, which is

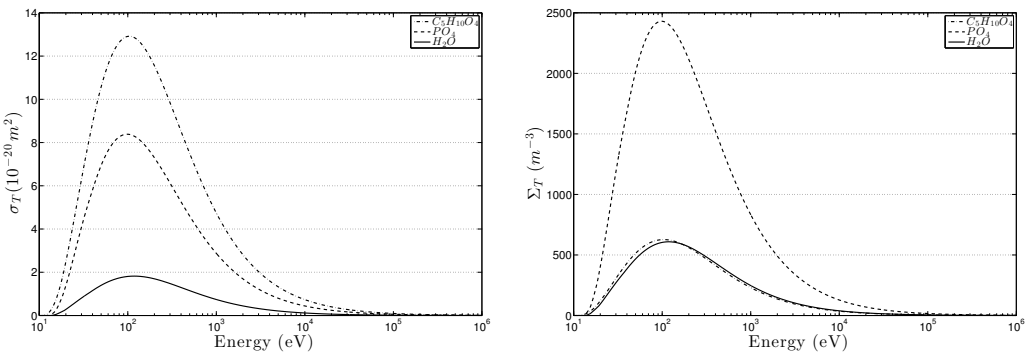

(a) Microscopic Cross Section (b) Macroscopic Cross Section

Figure 4.6: The Cross sections for the materials of the Phosphodiester Unit (2-dexorbose, Phosphate) and the water cross sections.

accounted for by the larger number of orbitals. As the cross section is a sum of the cross sections of the individual orbits, the DNA will have a larger cross section. The phosphate, is a small molecule that is much heavier than water giving it a density of nearly 5 $^{g}/_{cm^3}$. This increases the number density, and therefore, the macroscopic cross section. The ribose is less dense than water, but has more orbitals. To get the same number of orbitals for deoxyribose, there would have to be 5 water molecules. The phosphate would require 6+ water molecules. As mentioned above, only 1.2 water molecules could fit in the space of the phosphate. The code does not distinguish whether the ionization occurred in the phosphate or the deoxyribose. Figure 4.6 shows the microsopic and macroscopic cross sections for the three materials used in the simulation. The microscopic cross sections are proportional to the number of orbitals. The molecules with the highest number of orbitals have the highest cross sections. However, when the number density is factored in, the phosphate molecules have become the highest probability of ionization. Phosphate molecules are so dense that they far exceed that of other molecules. The water and ribose are on similar magnitudes, and water may be a good approximation for the deoxyribose but not the phosphate.

Table 4.1: The results of the simulations, showing the the ratio of double strand breaks to single strand breaks and the total ionizations per event for the water analog and the actual DNA material over the energies of common Auger emitters. The $50eV$ incident required more primaries to make the values statistically significant. At that energy, 1×10^7 events were run for DNA and 1×10^8 for water

	Water		**DNA**	
Energy (eV)	$\frac{\text{DSB}}{\text{SSB}}(\%)$	Ionizations ($\times 10^{-3}$)	$\frac{\text{DSB}}{\text{SSB}}(\%)$	Ionizations ($\times 10^{-3}$)
20	—	17.5 ± 7.5	—	55.3 ± 4.1
50	1.52 ± 0.59	45.2 ± 4.6	3.23 ± 1.72	115.9 ± 2.8
75	2.92 ± 1.09	67.8 ± 3.7	5.47 ± 2.31	167.7 ± 2.2
100	4.05 ± 0.84	88.2 ± 3.2	7.39 ± 1.74	217.1 ± 1.9
250	6.48 ± 0.40	203.2 ± 2.0	13.45 ± 0.92	537.2 ± 0.9
500	6.35 ± 0.23	445.7 ± 1.1	14.69 ± 0.62	1244.8 ± 0.4
750	5.82 ± 0.18	699.3 ± 0.7	14.21 ± 0.51	2047.8 ± 0.7
1000	5.43 ± 0.16	862.0 ± 0.4	13.39 ± 0.47	2704.3 ± 0.8

The number of ionizations might be elevated above the actual value. Only the ionization model accounts for the DNA materials. Excitation and scattering have the proper ratio to ionization when the water analog is used. When the DNA material is used, the number density of the phosphate would increase the probability of excitation and scattering proportionally to the number density. This leads to an artificial increase of number of ionization events in the phosphate volume. Another source of artificial increase in the ionizations in the phosphate is the volume given to the phosphate could be too small. The volume was calculated to be slightly larger than a sphere with a radius from the center of an oxygen to the center of the phosphate. This effect would be less pronounced, as any volume given to the phosphate would be taken from the ribose, increasing the number density and probability of ionization in the ribose.

Double strand breaks are more important than the number of ionizations. The ratio of double strand breaks as well as the ionizations presented in Figure 4.5 are shown in Table 4.1. The presence of double strand breaks beginning at $50eV$ and

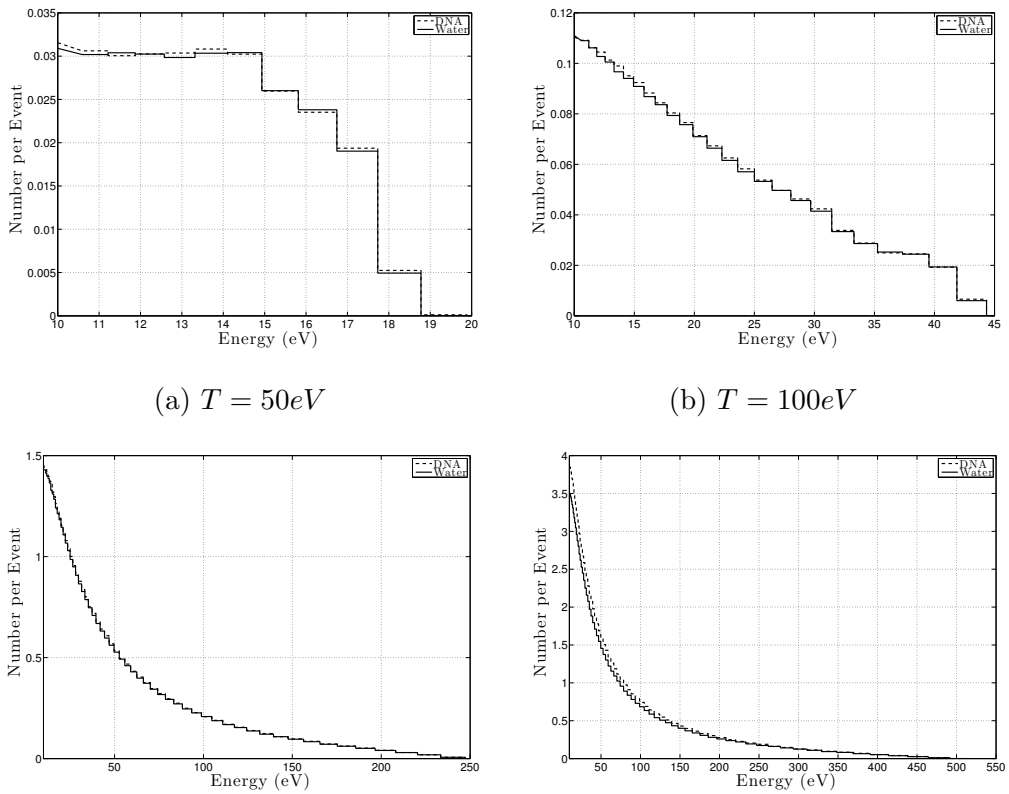

(a) $T = 50eV$ (b) $T = 100eV$

(c) $T = 500eV$ (d) $T = 1000eV$

Figure 4.7: The energy of the secondary electrons, scattered and ejected, from the two materials (DNA and Water) at primary energies of $50, 100, 500$ and $1000eV$. The values have been normalized to the number of events, in this case 1×10^6

higher corresponds well with experiment [5]. The DNA show marked improvements in the number of DSBs over water. Not only are ionizations in general more probable, the increased probability gives rise to more DSBs. This is simply a function of increased ionization probability with the DNA material. Figure 4.7 shows that the energies of the secondary electrons coming off DNA and water are very similar. At $100eV$ the DNA seems to have higher energy electrons than the water. This is likely contributing to the increase in DSBs in DNA. The higher energy electrons will

have a more energy they can deposit in the opposite strand causing a DSB. The discrepancy is highest over the energy range where the cross sections are the largest; only accentuating the effects of DNA.

Chapter 5

Conclusion

The assumption that water can serve as an analog for DNA in Monte Carlo simulations was tested. Geant4 was used as the simulation package because the design of the code allows easy addition of physics modules without the need to write the other supporting parts of Monte Carlo simulations. The current release of Geant4 can only handle water for low energy electron physics. To change the materials in the simulation another physics module needed to be added to handle a variety of materials, including phosphate and 2-dexoribose. Ionization drives the process of direct DNA damage (strand breaks), thus, only the ionization model was altered. The model chosen was the Binary-Encounter-Bethe (BEB) model developed by Rudd and Kim [14]. The geometry was built to represent a chromatin fiber, on the molecular level. The fiber was built by approximating the DNA backbone as an assembly of prisms. Each prism represented a 2-deoxyribose or a phosphate molecule. The chromatin fiber was surrounded by liquid water and irradiated by low energy ($\leq 1000eV$) electrons. The model was verified and validated by comparing the results to the existing model in Geant4, The Born Model. The simulation could not be validated against experiment because there are few experiments and the preparation of the DNA does not allow for free DNA that can only be affected by direct action [5].

The BEB model was found to produce fewer ionizations over the higher energies. This was due to the fact that the BEB allows lower orbitals, with higher binding energies, to be ionized. This deposits more energy and the secondary electrons have less energy and therefore, less probability of ionization. The model was determined to be accurate for the scope of this work. The BEB model is an approximate model and is not ideal for producing the energies of secondary electrons [14]. As the BEB model for water was compared to the BEB model for DNA, the total ionizations are not as crucial as the relative ionizations for water and DNA. The BEB model does produce same order of magnitude results. The test was performed over several energies: 20, 50, 75, 100, 250, 500, 750 and $1000eV$. The DNA proved to more susceptible to strand breaks than the water analog. This is a result of many things; most importantly is that the phosphate has a very high number density. Phosphate, with a phosphorous and four oxygen atoms, is a compact and heavy molecule. This increases the electron interaction probability making ionizations in the phosphate unit more probable per volume of DNA than for water. This increased probability leads to an increase in double strand breaks (DSBs); the most biologically important damage. The other factor working is the fact that ionization in phosphate has to be artificially increased, as the other processes were not scaled by the higher number density. This gives ionization an even greater chance of happening in phosphate than the calculations show. More work must be done to definitively say whether the water analog is a good approximation. However, the work indicates that water is not able to accurately represent DNA when simulating the effects of low energy electrons, specifically Auger electrons.

Chapter 6

Future Work

6.1 Model Improvements

The first improvements needs to be made by adding the excitation and scattering models that handle DNA materials. Scattering can be added using the independent atom method (IAM) [19]. This method assumes that each atom of the molecule scatters independently, multiple scattering is negligible, and any redistribution of electrons for molecular binding are ignored [19]. This method gives a differential cross section of the form:

$$\frac{d\sigma}{d\Omega} = \sum_{j=1}^{N} \frac{d\sigma^A}{d\Omega_j} + \sum_{i \neq j=1}^{N} f_i(\theta, k) f_j^*(\theta, k) \frac{\sin(sr_{ij})}{sr_{ij}} \tag{6.1}$$

where N is the number of atoms, θ is the scattering angle and $f_i(\theta, k)$ is the scattering amplitude due the i-th atom, s is the wave number, and r_{ij} is the internuclear distance between the i-th and j-th atoms. [19]. Much of the information for this can be determined using the GAMESS. Finding the scattering amplitude for each atom requires the partial wave analysis and solving the asymptotic radial Schrödingier equation with the static and polarization potentials.

Excitation is much more *ad hoc*; most theories are very sophisticated and require more calculations than is reasonable for this work [18]. Following the work of Nikjoo, et. al. [21] the excitation cross section can be approximated by:

$$[\sigma_{exc}]_{DNA} \approx [\sigma_{ion}] \left[\frac{\sigma_{exe}}{\sigma_{ion}}\right]_{water} \tag{6.2}$$

giving a simple order of magnitude approximation for the excitation cross section.

Deexcitation also needs to be added. Many of the ionizations come from inner shells; the process leaves a vacancy, in which an electron can fall releasing an x-ray or an Auger electron. This x-ray or Auger electron can go on to cause more ionizations, specifically in DNA as it was born in close proximity to the backbone. This could potentially increase the the number of double strand breaks. There exists an atomic deexcitation module in Geant4 but it is only applicable for free atoms [8]. The molecular energy levels can be quite different than atomic orbitals, and this discrepancy would lead to inaccuracies. The physics could be overloaded to accept the already available orbital information needed for the ionization model.

The issues with the geometry need to be fixed; having an electron trapped between volumes due to the small nature of the geometry makes simulations very difficult to execute en mass. A work-around for this must be found. A similar Geant4 geometry object, `G4PVReplica`, has a well documented problem that gives the same output. The developers have not fixed it but they have found a work-around by using an odd number of volumes, this work-around has not worked for the `G4AssemblyVolume`. Perhaps this will be fixed in the next release of Geant4; it is clearly a bug and has been submitted as such to the development team.

Another improvement would be the addition of nucleobases to the geometry; while it is simple, it was not necessary for this simulation. The extra material between the strands' backbones could reduce the number of strand breaks by attenuating the electrons. An ionization event in a base geometry would not result in a strand break

and would cause a loss of energy in the primary electron making it possible that it may not be able to cause an ionization in the strand. Also the angle would change making it likely that the electron might not pass through a PU. Scattering would have a similar effect. This would only help refine the simulation and may not make a large difference in the overall outcome.

This simulation only took into account the DNA damage done by direct action, which is important but not the only mode of DNA damage. Indirect action could be added to accurately simulate DNA in a biological environment. The Geant4-DNA team is working to include chemical diffusion and strand breaks, but these are not in the current release. This can be done through Monte Carlo, or by an approximation stating that a certain percentage of ionizations inside a volume result in a strand break [9]. This would provide a comprehensive simulation package for nanodosimetric calculations and would be able to characterize true damage done by incorporated Auger emitters or secondary radiation.

6.2 Other Particles

The addition of photon physics would greatly improve the simulation. Geant4 already includes low energy photon physics, including Rayleigh Scattering and the photoelectric effect, which dominate the low energy photon spectrum [8]. The models require atoms and do not work for molecules; while this would be a quick addition to the simulation, its accuracy would be suspect. Creating a way to incorporate molecular information would follow in a similar manner as was done for electrons. This physics might be easier to include, but the possibility has not been investigated.

Appendices

A Computer Specifications **4**

B GAMESS Input Files **5**

C GEANT Geometry Error **6**

Appendix A

Computer Specifications

System:

Mac Pro 5,1

Processor: 2 x 2.4 GHz 6-Core Intel Xenon

L2 Cash 256 kB per Core

L3 Cas 12 MB per Core

Memory: 24 GB 1333 MHz DDR3

Software:

Operating System: Mac OS X 10.8.3 Mountain Lion

GEANT Version: GEANT4.9.6.p01

Data: G4EMLOW6.32

GEANT Build Information:

CMake: Version 2.8.10

Complier: i686-apple-darwin11-llvm-gcc-4.2

Terminal: GNU bash, version 3.2.48(1) release

XQuartz: Version 2.7.4 (xorg-server 1.13.0)

Appendix B

GAMESS Input Files

Water Energy:

```
 $contrl scftyp=RHF runtyp=energy icharg=0
    mult=1 coord=zmt $end
 $system timlim=60  mwords=5 $end
 $basis gbasis=N311 ngauss=6 $end
 $guess guess=huckel $end
 $data
Water...RHF_STO-3G
Cnv  2

O
H  1  rOH
H  1  rOH  2  aHOH

rOH=0.9894194
aHOH=100.0270395
 $END
```

Phosphate Orbital Energy Decomposition:

```
!phosphate orbital decomp
 $contrl scftyp=rhf runtyp=eda $end
 $system timlim=3 $end
 $basis  gbasis=n311 ngauss=6 $end
 $guess  guess=huckel $end

 $lmoeda matom(1)=8 mcharg(1)=0 mmult(1)=1 $end
 $contrl nosym=1 $end
 $system mwords=8 $end

 $DATA
Title
C1
P    15.0    -1.97427     2.12256    -0.09723
O     8.0    -0.55508     2.04447    -0.80221
O     8.0    -1.85182     3.39603     0.84366
O     8.0    -1.96826     0.87728     0.88828
O     8.0    -3.15385     2.16112    -0.99903
H     1.0    -2.27265     4.17000     0.42495
H     1.0    -2.45931     0.13109     0.49648
H     1.0     0.15673     2.02336    -0.13698
 $END
```

2-Deoxiribose Energy:

```
!deoxyribose Energy
 $contrl scftyp=rhf runtyp=energy $end
 $system timlim=1 $end
 $basis  gbasis=n311 ngauss=6 $end
 $guess  guess=huckel $end

 $DATA
Title
C1
O     8.0    -0.57985     2.82851    -0.56428
C     6.0    -1.68696     1.91614    -0.40336
C     6.0    -1.13223     0.71233     0.35027
C     6.0     0.27552     0.64848    -0.19029
C     6.0     0.63470     2.11490    -0.28659
C     6.0    -2.84735     2.58587     0.33699
O     8.0    -3.44939     3.62544    -0.43599
O     8.0    -1.86203    -0.47141     0.08413
H     1.0    -2.49906     3.04485     1.26783
H     1.0    -3.62829     1.85745     0.57595
H     1.0    -2.01542     1.63195    -1.41110
H     1.0    -1.11900     0.89142     1.43216
H     1.0    -1.38763    -1.21184     0.50096
H     1.0     0.96004     0.07852     0.44436
H     1.0     0.28372     0.17963    -1.18203
H     1.0     1.03045     2.48834     0.66401
H     1.0     1.36839     2.31624    -1.07212
H     1.0    -3.51808     3.31127    -1.35365
 $END
```

Appendix C

Geant4 Geometry Error

```
-------- WWWW ------- G4Exception-START -------- WWWW -------
*** G4Exception : GeomNav1002
      issued by : G4Navigator::ComputeStep()
Track stuck or not moving.
          Track stuck, not moving for 10 steps
          in volume -Target- at point (1.69028e-06,1.31183e-05,-3.37702e-05)
          direction: (-0.202246,-0.281709,-0.937943).
          Potential geometry or navigation problem !
          Trying pushing it of 1e-07 mm ...Potential overlap in geometry!

*** This is just a warning message. ***
-------- WWWW -------- G4Exception-END --------- WWWW -------
```

References

[1] Alexandre, A., Tavares, S., Manuel, J., and Tavares, R. S. "^{99m}Tc Auger Electrons for Targeted Tumor Therapy: A Review". *International Journal of Radiation Biology 86*, 4 (2010), 261–270.

[2] Bernal, M., and Liendo, J. "An Investigation on the Capabilities of the PENELOPE MC Code in Nanodosimetry". *Medical Physics 36*, 2 (2009), 620–625.

[3] Collaboration, G., Agostinelli, S., and et al. "Geant4: A Simulation Toolkit". *Nuclear Instruments and Methods A 506*, 25 (2003).

[4] Dickerson, R. E., Drew, H. R., Conner, B., Wing, R., Fratini, A., and Kopka, M. "The Anatomy of A-, B-, and Z-DNA". *Science, New Series 216*, 4545 (April 1982), 475–485.

[5] Folkard, M., Prise, K., Vojnovic, B., Davies, S., Roper, M., and Michael, B. "Measurement of DNA Damage by Electrons with Energies Between 25 and 4000 eV'. *International journal of radiation biology 64*, 6 (1993), 651–658.

[6] Friedland, W., Jacob, P., Bernhardy, P., Paretzke, H., and Dingfelder, M. "Simulation of DNA Damage after Proton Irradiation". *Radiation Research 159* (2003), 401–410.

[7] Gardner, E. J., Simmons, M. J., and Sunstand, D. P. *Principles of Genetics*, 8th ed. John Wiley and Sons, Inc., 1991.

[8] Geant4 Collaboration. Geant4 User's Guide of Application Developers, November 2012.

[9] Grosswendt, B. "Low-Energy Monte Carlo and W-Values". In *Monte Carlo Transport of Electrons and Photons*, T. M. Jenkins, W. R. Nelson, and A. Rindi, Eds. Plenum Press, 1888, ch. 15, pp. 344 – 360.

[10] Hall, E. J. *Radiobiology for the Radiologist*, 4th ed. J.B. Lippincott Company, 227 East Washington Square, Philadelphia, PA 19106-3780, 1994.

[11] Hwang, W., Kim, Y.-K., and Rudd, Y. "New Model for Electron-Impact Ionization Cross Sections of Molecules". *Journal of Chemical Physics 104*, 8 (February 1996), 2956–2966.

[12] Incerti, S., Baldacchino, G., Bernal, M., Capra, R., Champion, C., Francis, Z., Guatelli, S., Guèye, P., Mantero, A., Mascialino, B., Moretto, P., Nieminen, P., Rosenfeld, A., Villagrasa, C., and Zacharatou, C. "The Geant4-DNA Project". *International Journal of Modeling, Simulation, and Scientific Computing 1* (2010), 157–178.

[13] Kereiakes, J., Rao, D., Sastry, K., and Howell, R. "Auger Electron Dosimetry". *Medical Physics 19*, 6 (1992).

[14] Kim, Y.-K., and Rudd, M. "Binary-Encounter-Dipole Model for Electron-Impact Ionization". *Physical Review A 50*, 5 (November 1994), 3954–3967.

[15] Klug, W. S., Cummings, M. R., and Spencer, C. A. *Concepts of Genetics*, eighth ed. Pearson Benjamin Cummings, San Francisco, 2005.

[16] Leslie, A. G. W., Arnott, S., Chandrasekaranand, R., and Ratliff, R. L. "Polymorphism of DNA Double Helices". *Journal of Molecular Biology 143*, 1 (October 1980), 49–72.

[17] Luger, K., Mader, A., Richmond, R., Sargent, D., and Richmond, T. "Crystal Structure of the Nucleosome Core Particle at 2.8 åResolution". *Nature 389*, 6648 (1997), 251–260.

[18] Märk, T., and Dunn, G., Eds. *Electron Impact Ionization*. Springer-Verlag Wien-New York, 1985.

[19] Moėjko, P., and Sanche, L. "Cross Section Calculations for Electron Scattering from DNA and RNA Bases". *Radiation Environment Biophysics 42* (September 2003), 201–211.

[20] Nikjoo, H., and Lindborg, L. "RBE of Low Energy Electrons and Photons". *Physics in Medicine and Biology 55* (April 2010), R65–R109.

[21] Nikjoo, H., O'Neill, P., Terrissol, M., and Goodhead, D. T. "Quantitative Modelling of DNA Damage using Monte Carlo Track Structure Method". *Radiation and Environmental Biophysics 38*, 1 (May 1999), 31–38.

[22] Robinson, P. J. J., Fairall, L., Huynh, V. A. T., and Rhodes, D. "EM Measurements Define the Dimensions of the "30-nm" Chromatin Fiber: Evidence for a Compact, Interdigitated Structure". *Medical Research Council Laboratory of Molecular Biology 103*, 17 (April 2006), 6506–6511.

[23] Roeske, J., Aydogan, B., Bardies, M., and Humm, J. "Small-Scale Dosimetry: Challenges and Future Directions". *Seminars in Nuclear Medicine 38*, 5 (2008), 367 – 383.

[24] Saenger, W. *Principles of Nucleic Acid Structure*. Springer-Verlag, 1984.

[25] Schmidt, M., Baldridge, K., Boatz, J., Elbert, S., Gordon, M., Jenson, J., Koseki, S., Matsunaga, N., Nguyen, K., Su, S., Windus, T., Dupus, M., and Montgomery, J. "General Atomic and Molecular Electronic Structure System". *Journal of Computational Chemistry 14* (1993), 1347–1363.

[26] Swarts, S. G., Sevilla, M. D., Becker, D., Tokar, C. J., and Wheeler, K. T. "Radiation-Induced DNA Damage as a Function of Hydration: I. Release of Unaltered Bases". *Radiation Research 129*, 3 (March 1992), 333–344.

[27] Turner, J. E. *Atoms, Radiation, and Radiation Protection*, 3rd ed. Wiley-VCH GmbH and Co. KGaA, 2007.

[28] Villagrasa, C., Francis, Z., and Incerti, S. "Physical Models Implemented in the Geant4-DNA Extension of the Geant-4 Toolkit for Calculating Initial Radiation Damage at the Molecular Level". *Radiation Protection Dosimetry 143*, 2-4 (December 2011), 214–218.

[29] Watson, J. D., Baker, T. A., Bell, S. P., Gann, A., Levine, M., and Losick, R. *Molecular Biology of the Gene*, 5 th ed. Pearson Education inc, 1301 Sansome Street, San Franciso, CA 94111, 2004.

[30] Wheeler, R. DNA Structure Key Labelled. `https://upload.wikimedia.org/wikipedia/commons/thumb/4/4c/DNA_Structure%2BKey%2BLabelled.pn_NoBB.png/615px-DNA_Structure%2BKey%2BLabelled.pn_NoBB.png`, April 2011.

[31] Widom, J. "A Relationship Between the Helical Twist of DNA and the Ordered Positioning of Nucleosomes in All Eukaryotic Cells". *Proceedings of the National Academy of Sciences 89*, 3 (1992), 1095–1099.

[32] Wing, R., Drew, H., Takano, T., Broka, C., Tanaka, S., Itakura, K., and Dickerson, R. E. "Crystal Strucutre Analysis of a Complete Turn of B-DNA". *Nature 287*, 5784 (October 1980), 755 – 758.